

# Tuning Frictional Properties of Kirigami Altered Graphene Sheets using Molecular Dynamics and Machine Learning

*Designing a Negative Friction Coefficient*

Mikkel Metzsch Jensen



Thesis submitted for the degree of  
Master in Computational Science: Materials Science  
60 credits

Department of Physics  
Faculty of mathematics and natural sciences

UNIVERSITY OF OSLO

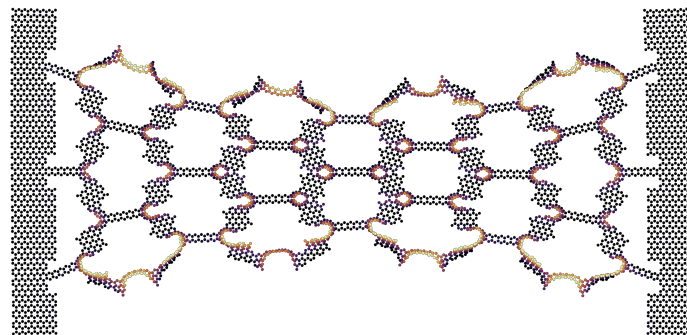
Spring 2023



# Tuning Frictional Properties of Kirigami Altered Graphene Sheets using Molecular Dynamics and Machine Learning

*Designing a Negative Friction Coefficient*

Mikkel Metzsch Jensen





© 2023 Mikkel Metzsch Jensen

Tuning Frictional Properties of Kirigami Altered Graphene Sheets using Molecular Dynamics and Machine Learning

<http://www.duo.uio.no/>

Printed: Reprocentralen, University of Oslo

# Abstract

Abstract.



# Acknowledgments

Acknowledgments.



# List of Symbols

$F_N$  Normal force (normal load)



# Acronyms

**CM** Center of Mass. 11

**FFM** Friction Force Microscopes. 9

**MD** Molecular Dynamics. 2, 3, 9

**ML** Machine Learning. 2, 3

**SFA** Surface force apparatus. 9



# Contents

|                   |                                    |           |
|-------------------|------------------------------------|-----------|
| <b>1</b>          | <b>Introduction</b>                | <b>1</b>  |
| 1.1               | Motivation . . . . .               | 1         |
| 1.2               | Goals . . . . .                    | 3         |
| 1.3               | Contributions . . . . .            | 3         |
| 1.4               | Thesis structure . . . . .         | 3         |
| <b>I</b>          | <b>Background Theory</b>           | <b>5</b>  |
| <b>II</b>         | <b>Simulations</b>                 | <b>7</b>  |
| <b>2</b>          | <b>Defining the system</b>         | <b>9</b>  |
| 2.1               | Region definitions . . . . .       | 9         |
| 2.2               | Numerical procedure . . . . .      | 11        |
| 2.3               | Creating the sheet . . . . .       | 12        |
| 2.3.1             | Graphene . . . . .                 | 12        |
| 2.3.2             | Indexing . . . . .                 | 13        |
| 2.3.3             | Removing atoms . . . . .           | 13        |
| 2.4               | Kirigami patterns . . . . .        | 15        |
| 2.4.1             | Tetrahedron . . . . .              | 15        |
| 2.4.2             | Honeycomb . . . . .                | 17        |
| 2.4.3             | Random walk . . . . .              | 17        |
| 2.4.3.1           | Fundamentals . . . . .             | 18        |
| 2.4.3.2           | Spacing of walking paths . . . . . | 18        |
| 2.4.3.3           | Bias . . . . .                     | 19        |
| 2.4.3.4           | Stay or break . . . . .            | 20        |
| 2.4.3.5           | Deployment schemes . . . . .       | 21        |
| 2.4.3.6           | Validity . . . . .                 | 22        |
| 2.4.3.7           | Random walk examples . . . . .     | 23        |
| <b>Appendices</b> |                                    | <b>25</b> |
| <b>Appendix A</b> |                                    | <b>27</b> |
| <b>Appendix B</b> |                                    | <b>29</b> |
| <b>Appendix C</b> |                                    | <b>31</b> |



# Chapter 1

## Introduction

**Structure of Motivation section:**

1. Introduce and motivate friction broadly.
2. Motives for friction control using a grasping robot as example.
3. Analog to gecko feet where adhesive properties are turned on and off.
4. Interest in origin of friction through nanoscale studies which further motivates the use of MD.
5. Intro to metamaterials and the use of kirigami designs,
6. How to optimize kirigami designs with reference to Hanakata and motivating the use of ML.
7. Out-of-plane buckling motivates the use of kirigami for frictional properties.

Does some of the latter paragraphs belong to the approach section?

### 1.1 Motivation

Friction is a fundamental force that takes part in most of all interactions with physical matter. Even though the everyday person might not be familiar with the term *friction* we recognize it as the inherent resistance to sliding motion. Some surfaces appear slippery and some rough, and we know intuitively that sliding down a snow covered hill is much more exciting than its grassy counterpart. Without friction, it would not be possible to walk across a flat surface, lean against the wall without falling over or secure an object by the use of nails or screws [p. 5] [1]. It is probably safe to say that the concept of friction is integrated in our everyday life to such an extent that most people take it for granted. However, the efforts to control friction dates back to the early civilization (3500 B.C.) with the use of the wheel and lubricants to reduce friction in translational motion [2]. Today, friction is considered a part of the wider field *tribology* derived from the Greek word *Tribos* meaning “rubbing” and includes the science of friction, wear and lubrication [2]. The most compelling motivation to study tribology is ultimately to gain full control of friction and wear for various technical applications. Especially, reducing friction is of great interest as this has tremendous advantages for energy efficiency. It has been reported that tribological problems have a significant potential for economic and environmental improvements [3]:

“On global scale, these savings would amount to 1.4% of the GDP annually and 8.7% of the total energy consumption in the long term.” [4].

On the other hand, the reduction of friction is not the only sensible application for tribological studies. Controlling frictional properties, besides minimization, might be of interest in the development of a grasping robot where a finetuned object handling is required. While achieving a certain “constant” friction response is readily obtained through appropriate material choices during manufacturing, we are yet to unlock the capabilities to alter friction dynamically on the go. One example from nature inspiring us to think along these lines are the gecko feet. More precisely, the Tokay gecko has received a lot of attention in scientific studies aiming to unravel the underlying

mechanism of its “toggable” adhesion properties. Although geckos are able to produce large adhesive forces, they retain the ability to remove their feet from an attachment surface at will [5]. This makes the gecko able to achieve a high adhesion on the feet when climbing a vertical surface while lifting it for the next step remains relatively effortless. For a grasping robot we might consider an analog frictional concept of a surface material that can change from slippery to rough on demand depending on specific tasks.

In the recent years an increasing amount of interest has gone into the studies of the microscopic origin of friction, due to the increased possibilities in surface preparation and the development of nanoscale experimental methods. Nano-friction is also of great concern for the field of nano-machining where the frictional properties between the tool and the workpiece dictates machining characteristics [3]. With concurrent progress in computational power and development of Molecular Dynamics (MD), numerical investigations serve as an extremely useful tool for getting insight into the nanoscale mechanics associated with friction. This simulation based approach can be considered as a “numerical experiment” enabling us to create and probe a variety of high complexity systems which are still out of reach for modern experimental methods.

In materials science such MD-based numerical studies have been used to explore the concept of so-called *metamaterials* where material compositions are designed meticulously to enhance certain physical properties [6][7][8][9][10][11]. This is often achieved either by intertwining different material types or removing certain regions completely. In recent papers by Hanakata et al. [6](2018) [7](2020) numerical studies have showcased that mechanical properties of a graphene sheet, in this case yield stress and yield strain, can be altered through the introduction of so-called *kirigami* inspired cuts into the sheet. Kirigami is a variation of origami where the paper is cut additionally to being folded. While these methods originate as an art form, aiming to produce various artistic objects, they have proven to be applicable in a wide range of fields such as optics, physics, biology, chemistry and engineering [12]. Various forms of stimuli enable direct 2D to 3D transformations through folding, bending, and twisting of microstructures. While original human designs have contributed to specific scientific applications in the past, the future of this field is highly driven by the question of how to generate new designs optimized for certain physical properties. However, the complexity of such systems and the associated design space makes for seemingly intractable problems ruling out analytic solutions.

Earlier architecture design approaches such as bioinspiration, looking at gecko feet for instance, and Edisonian, based on trial and error, generally rely on prior knowledge and an experienced designer [9]. While the Edisonian approach is certainly more feasible through numerical studies than real world experiments, the number of combinations in the design space rather quickly becomes too large for a systematic search, even when considering the simulation time on modern day hardware. However, this computational time constraint can be relaxed by the use of machine learning (ML) which have proven successful in the establishment of a mapping from the design space to physical properties of interest. This gives rise to two new styles of design approaches: One, by utilizing the prediction from a trained network we can skip the MD simulations all together resulting in an *accelerated search* of designs. This can be further improved by guiding the search accordingly to the most promising candidates, as for instance done with the *genetic algorithm* which suggest new designs based on mutation and crossing of the best candidates so far. Another, even more sophisticated approach, is through generative methods such as *Generative Adversarial Networks* (GAN). By working with a so-called *encoder-decoder* network structure, one can build a model that reverses the prediction process. That is, the model predicts a design from a set of physical target properties. In the papers by Hanakata et al. both the *accelerated search* and the *inverse design* approach was proven successful to create novel metamaterial kirigami designs with the graphene sheet.

Hanakata et al. attributes the variety in yield properties to the non-linear effects arising from the out-of-plane buckling of the sheet. Since it is generally accepted that the surface roughness is of great importance for frictional properties it can be hypothesized that the kirigami cut and stretch procedure can also be exploited for the design of frictional metamaterials. For certain designs we might hope to find a relationship between stretching of the sheet and frictional properties. If significant, this could give rise to a variability of the friction response beyond manufacturing material choice. For instance, the grasping robot might apply such a material as artificial skin for which stretching or relaxing of the surface could result in a changeable friction strength; Slippery and smooth when in contact with people and rough and firmly gripping when moving heavy objects. In addition, a possible coupling between stretch and the normal load through a nanomachine design would allow for an altered friction coefficient. This invites the idea of non-linear friction coefficients which might in theory also take on negative values given the right response from stretching. The latter would constitute an extremely rare property. This has (**only?**) been reported indirectly for bulk graphite by Deng et al. [13] where the friction kept increasing during the unloading phase. **Check for other cases and what I can really say here.**

To the best of our knowledge, kirigami has not yet been implemented to alter the frictional properties of a nanoscale system. In a recent paper by Liefferink et al. [14](2021) it is reported that macroscale kirigami can be used to dynamically control the macroscale roughness of a surface through stretching which was used to change the frictional coefficient by more than one order of magnitude. This supports the idea that kirigami designs can in fact be used to alter friction, but we believe that taking this concept to the nanoscale regime would involve a different set of underlying mechanisms and thus contribute to new insight in this field.

## 1.2 Goals

In this thesis we investigate the possibility to alter and control the frictional properties of a graphene sheet through application of kirigami inspired cuts and stretching of the sheet. With the use of MD simulations we evaluate the friction properties under different physical conditions in order to get insight into the prospects of this field. By evaluating variations of two kirigami inspired patterns and a series of random walk generated patterns we create a dataset containing information of the frictional properties associated with each design under different load and stretch conditions. We apply ML to the dataset and use an accelerated search approach to optimize for different properties of interest. The subtask of the thesis are presented more comprehensively in the following.

1. Define a sheet indexing that allows for a unique mapping of patterns between a hexagonal graphene lattice representation to a matrix representation suited for numerical analysis.
2. Design a MD simulation procedure to evaluate the frictional properties of a given graphene sheet under specified physical conditions such as load, stretch, temperature etc.
3. Find and implement suitable kirigami patterns which exhibit out-of-plane buckling under tensile load. This includes the creation of a framework for creating variations within each pattern class. Additionally create a procedure for generating different styles of random walk patterns.
4. Perform a pilot study of a representative subset of patterns in order to determine appropriate simulation parameters to use for the further study along with an analysis of the frictional properties shown in the subset.
5. Create a dataset consisting of the chosen kirigami variations and random walk patterns and analyse data trends.
6. Train a neural network to map from the design space to physical properties such as mean friction, maximum friction, contact area etc. and evaluate the performance.
7. Perform an accelerated search optimizing for interesting frictional properties using the ML model. This should be done both through the pattern generation procedures and by following a genetic algorithm approach.
8. Use the most promising candidates from the accelerated search to investigate the prospects of creating a nanomachine setup which exhibits a negative friction coefficient.
9. Study certain designs of interest with the scope of revealing underlying mechanism. This includes simple correlation analysis but also a visualization of feature and gradient maps of the ML network.

Is the list of subtask too specific? Some of the details here might be better suited for the thesis structure section.

## 1.3 Contributions

What did I actually achieve

## 1.4 Thesis structure

How is the thesis structured.



# Part I

# Background Theory



## **Part II**

# **Simulations**



# Chapter 2

## Defining the system

The definition of the system plays a crucial role as it essentially sets the scene for the whole study. With the general goal of investigating the frictional behaviour of a graphene sheet as we alter it through kirigami cuts and stretch, two different approaches were considered as sketched in Fig. 2.1. One approach is simply to mimic a FFM type experiment as done in most other numerical studies of friction. In this case, we can probe the graphene sheet, resting on a substrate, with some sort of indenting tip connected to a moving body representing a cantilever setup. Friction is then measured by making the tip scan across the graphene surface. This setup allows for a variety of tip shapes and sizes, and alternatively it could be broadened a flat surface making the setup resemble a SFA experiment. However, this approach seemingly calls for a fixed amount of stretching of the graphene sheet as it is pre-stretched before being attached to the substrate. Another option is therefore to attach the graphene sheet to the moving body instead. The key difference is then, that it introduces some sort of nanomachine in the moving body which converts a normal load into a stretching motion. This gives more design room to utilize any stretch-related friction effects that require a dynamical changing of the stretch amount as opposed to only being applied to keep the sheet at a certain stretch amount throughout the loading.

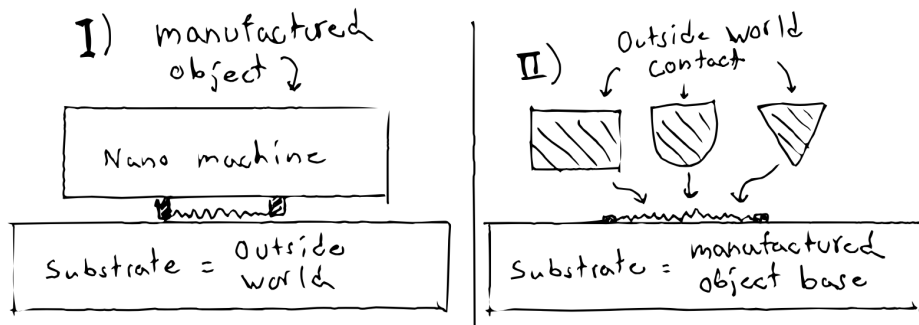


Figure 2.1: TMP System variations

Hence, using the second option our system of choice consists of two separate parts: A 2D graphene sheet and a 3D Silicon “bulk” substrate. Note, that we do attempt to model the nanomachine explicitly in this study, but we will consider the prospects of adding this in ??.

### 2.1 Region definitions

Despite having two distinct parts of the simulation, the sheet and the substrate, we provide a further subdivision into specific regions according to their functionality in the MD simulations. We denote the start and end regions of the sheet, with respect to one direction, as so-called *pull blocks*, which is reserved for the application of normal load, stretching and dragging of the sheet and applying the thermostat. The remaining *inner sheet* is left for the kirigami cuts and simulated as an *NVE* ensemble. The pull blocks are equally split between a thermostat part and a rigid part. The rigid part is part of the thermostat during an initial relaxation period before it is

then made rigid for the final duration of the simulation. Note that the rigid parts on both sides of the sheet is then considered as a single rigid object even though they are physically separated. This means that all force interactions on these parts will be applied as a common average making the move in total synchronization. The substrate is equally divided into three parts: The *upper layers* (*NVE*) responsible for the sheet-substrate interaction, the *middle layers* being a thermostat (*NVT*), and the *bottom layers* being frozen, made rigid and fixed, in the initial lattice structure to ensure that the substrate stays in place. In Fig. 2.2 the system is displayed with colors matching the three distinct roles:

1. Red: *NVE* parts which is governing the frictional behaviour of interest.
2. Green: Thermostats (*NVT*) surrounding the *NVE* parts in order to modify the temperature without making disturbing changes to the interaction of the sheet and substrate.
3. Blue: Parts that is initially or eventually turned in to rigid objects. For the substrate this refers to an additionally fixation as well.

The total system size, without cuts in the sheet, is roughly 27k atoms, while the full sheet measure  $\sim 130 \times 163 \text{ \AA}$ . The precise numbers and region subdivision is shown for the system atom count in Table 2.1 and the sheet dimensions in Table 2.2.

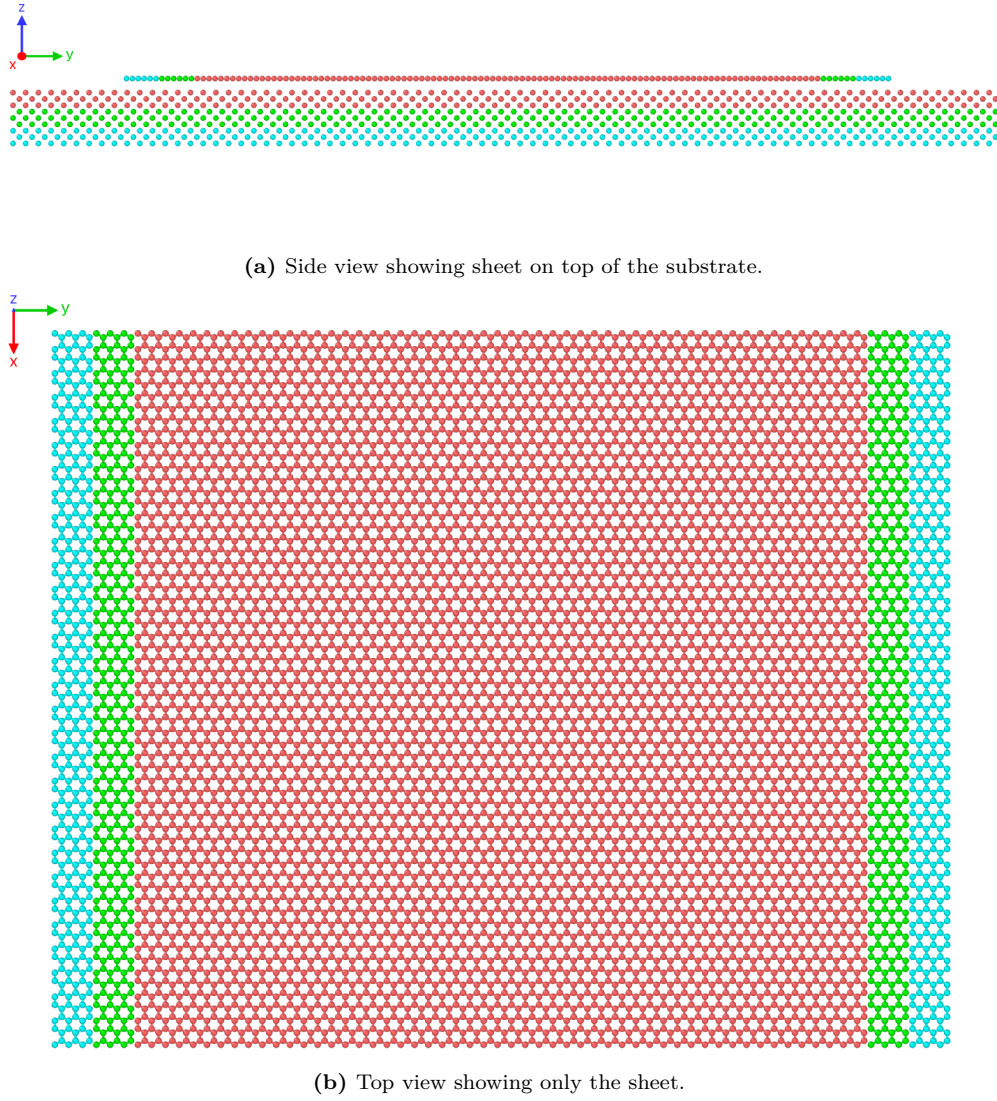


**Figure 2.2:** System configuration colorized to indicate *NVE* parts (red), thermostat parts (green) and rigid parts (blue).

**Table 2.1:** Amount of atoms in the various system regions in the case of no cutting applied to the sheet.

| Region    | Total | Sub region  | Sub total | NVE   | NVT  | Rigid |
|-----------|-------|-------------|-----------|-------|------|-------|
| Sheet     | 7800  | Inner sheet | 6360      | 6360  | 0    | 0     |
|           |       | Pull blocks | 1440      | 0     | 720  | 720   |
| Substrate | 19656 | Upper       | 6552      | 6552  | 0    | 0     |
|           |       | Middle      | 6552      | 0     | 6552 | 0     |
|           |       | Bottom      | 6552      | 0     | 0    | 6552  |
| All       | 27456 |             |           | 12912 | 7272 | 7272  |

**Table 2.2:** Sheet dimensions comparing the full sheet to its subdivisions: inner sheet and pull blocks.

| Group       | $x, y$ -dim                         | dim [Å]                                    | Area [Å <sup>2</sup> ] |
|-------------|-------------------------------------|--|------------------------|
| Full sheet  | $x_S \times y_S$                    | $130.029 \times 163.219 \text{ Å}$         | $21,223.203$           |
| Inner sheet | $x_S \times 81.40 \%_{y_s}$         | $130.029 \times 132.853 \text{ Å}$         | $17,274.743$           |
| Pull blocks | $2 \times x_S \times 9.30 \%_{y_s}$ | $2 \times 130.029 \times 15.183 \text{ Å}$ | $2 \times 1,974.230$   |

## 2.2 Numerical procedure

The numerical procedure related to the measurement of friction can be arranged into the following steps. Some steps have been given a duration denoted in parentheses in units of ps,  $10^{-12}$  seconds.

- 1. Relaxation** (15 ps): The sheet and substrate are relaxed for 15 ps after being added in their crystalline form with a separation distance of 3 Å which was found to be a reasonable estimate for the equilibrium distance at the temperature range of interest. The sheet is constrained under three hard spring forces, all with spring constant  $10^5 \text{ eV/Å}^2 \sim 1.6 \times 10^6 \text{ N/m}$ : One spring attaches the sheet center of mass (CM) to its original position, preventing any drift. The remaining two springs are attached to the pull block ends, to their initial CM position respectively, to prevent rotation. In principle, it would be sufficient to fixate just one of the ends in order to stop rotation, but we fixate both ends for the sake of symmetry. During the relaxation phase the pull blocks are made rigid with respect to the z-direction only (perpendicular to the sheet). That is, all the forces in the z-direction are summed up and distributed on the pull blocks as a single external force, while it is free to expand and contract in the x-y-plane. This is mainly to ensure that it achieves the correct lattice spacing according to the temperature of the system. For the following phases the rigid parts of the pull block are in fact rigid with respect to all directions. The spring forces are terminated after the relaxation phase.
- 2. Stretch:** The sheet is stretched by separating the two opposing rigid parts of the pullblock at constant velocity until the desired stretch amount is met. The duration of this phase is thus controlled by the *stretch speed* and *stretch amount* parameters.
- 3. Pause** (5 ps): The sheet is relaxed for 5 ps after the stretch procedure to ensure that the sheet is stable and equilibrated after the applied stretch deformation.
- 4. Normal load** (5 ps): The normal load is applied to the rigid parts of the pull blocks. Initially a viscous damping force,  $F = -\gamma v$ , is added to the sheet to resist the rapid acceleration of the sheet and prevent a hard impact between the sheet and substrate. The damping coefficient is set to  $\gamma = 8 \times 10^{-4} \text{ nN/(m/s)}$  and terminated after 0.5 ps as this was visually found to be suitable for the extreme load cases of our intended range of normal force. The remaining 4.5 ps devoted as a relaxation phase.
- 5. Sliding:** A virtual atom is introduced into the simulation which exclusively interacts with the rigid parts of the pull through a spring force with variable spring constant  $K$  in the x-y-plane. The z-direction is not affected by the spring force and is purely governed by the balance between normal load and the normal response from the sheet-substrate interaction. The virtual atom is immediately given a constant velocity, corresponding to a the *sliding speed* parameter, which make the sliding force increase proportional to

$\propto K(vt)^2$  for sliding speed  $v$ . An infinite spring constant can also be chosen for which the spring is omitted and the pull blocks are moved rigidly with the constant speed according to the sliding speed.

In order to prevent rupturing, or detachment, of the sheet we monitor the nearest neighbours for each atom throughout the simulation. At the initial timestep the three nearest neighbours (at distance 1.42 Å) of all graphene atoms is recorded. If any of these nearest neighbours exceeds a threshold distance of 4 Å, indicating a bond breakage, this is marked as a rupture and we halt the simulation early. Thus, we ensure that no wear is allowed for the sheet. The substrate is way more robust and by running test simulation of high load and sliding speed we confirmed visually that no wear is occurring in the vicinity of the conditions used in the study.

## 2.3 Creating the sheet

We are going to create a 2D sheet graphene sheet.

### 2.3.1 Graphene

Graphene is a single layer of carbon atom, graphite is the bulk, arranged in a hexagonal lattice structure. We can describe the 2D crystal structure in terms of its primitive lattice vector and a basis. That is we populate each lattice site by the given basis and translate it to fill the whole plane by any linear combination of the lattice vectors

$$\mathbf{T}_{mn} = m\mathbf{a}_1 + n\mathbf{a}_2, \quad m, n \in \mathbb{N}.$$

For graphene we have the primitive lattice vectors

$$\mathbf{a}_1 = a \left( \frac{\sqrt{3}}{2}, -\frac{1}{2} \right), \quad \mathbf{a}_2 = a \left( \frac{\sqrt{3}}{2}, \frac{1}{2} \right), \quad |\mathbf{a}_1| = |\mathbf{a}_2| = 2.46 \text{ Å}.$$

Notice that we deliberately excluded the third coordinate as we only consider a single graphene layer or not the bulk graphite consisting of multiple layers stacked on top of each other. The basis is

$$\left\{ (0,0), \frac{a}{2} \left( \frac{1}{\sqrt{3}}, 1 \right) \right\}$$

It turns out that the spacing between atoms is equal for all pairs with an interatomic distance

$$\left| \frac{a}{2} \left( \frac{1}{\sqrt{3}}, 1 \right) \right| \approx 1.42 \text{ Å}.$$

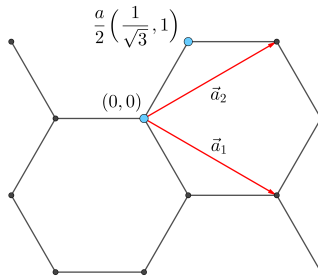


**Figure 2.3:** Graphene crystal structure with basis.

### 2.3.2 Indexing

In order to define the cut patterns applied to the graphene sheet we need to define an indexing system. We must ensure that this gives an unique description of the atoms as we eventually want to pass a binary matrix, containing 0 for removed atoms and 1 for present atoms, that uniquely describes the sheet. We do this by letting the x-coordinate point to zigzag chains and the y-coordinate to the position along that chain. This is illustrated in figure Fig. 2.4. Other solutions might naturally invoke the lattice vectors, but as these are used to translate between similar basis atoms unfortunate duality is introduced as one need to include the basis atom of choice into the indexing system. Additionally, we want a system where the indexes reflect the relative physical position of neighbours . That is, atom  $(i, j)$  is in the proximity of  $\{(i + 1, j), (i - 1, j), (i, j + 1), (i, j - 1)\}$ . However, only three of them is categorized as nearest neighbours due to the hexagonal structure of the lattice. While  $(i, j \pm 1)$  is always a nearest neighbour the neighbour in the x-direction flip sides when incrementing either x- or y-coordinate. That is the nearest neighbours (NN) is decided as

$$\begin{aligned} (i + j) \text{ is even} &\rightarrow \text{NN} = \{(i - 1, j), (i, j + 1), (i, j - 1)\}, \\ (i + j) \text{ is odd} &\rightarrow \text{NN} = \{(i + 1, j), (i, j + 1), (i, j - 1)\}. \end{aligned} \quad (2.1)$$

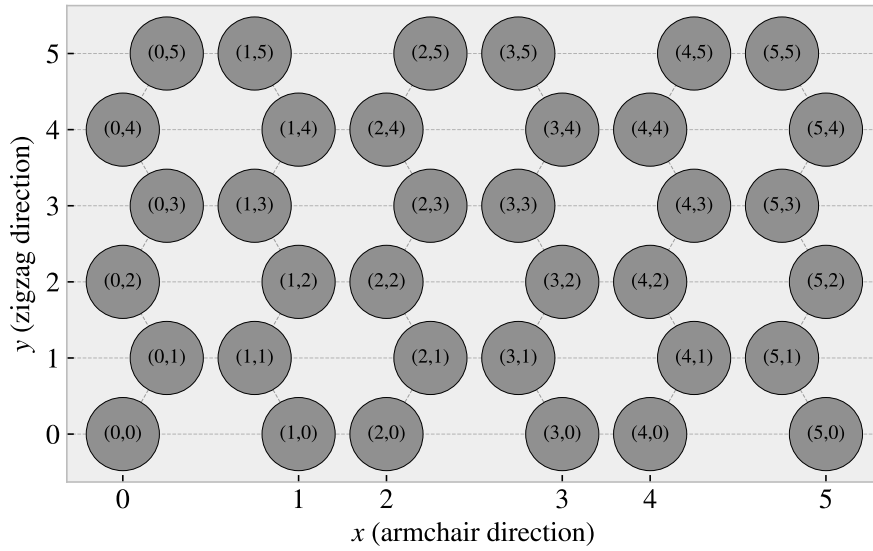


**Figure 2.4:** Graphene atom indexing

### 2.3.3 Removing atoms

As a mean to ease the formulation of cut patterns we introduce pseudo center element in each gap of the hexagonal honeycombs, see figure Fig. 2.5.

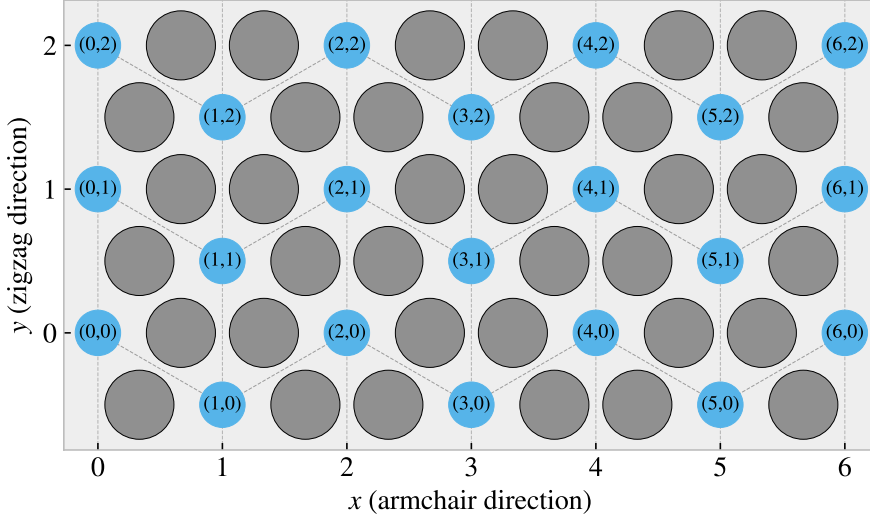


**Figure 2.5:** Graphene center indexing

Similar to the case of the indexing for the carbon atoms themselves the nearest neighbour center elements alternate with position, this time only along the x-coordinate index. Each center element has six nearest neighbours, in clock wise direction we can denote them: “up”, “upper right”, “lower right”, “down”, “lower left”, “upper left”. The “up” and “down” is always accessed as  $(i, j \pm 1)$ , but for even  $i$  the  $(i + 1, j)$  index corresponds to the “lower right” neighbour while for odd  $i$  this corresponds to the “upper right” neighbour. This shifting applies for all left or right neighbours and the full neighbour list is illustrated in Fig. 2.6.

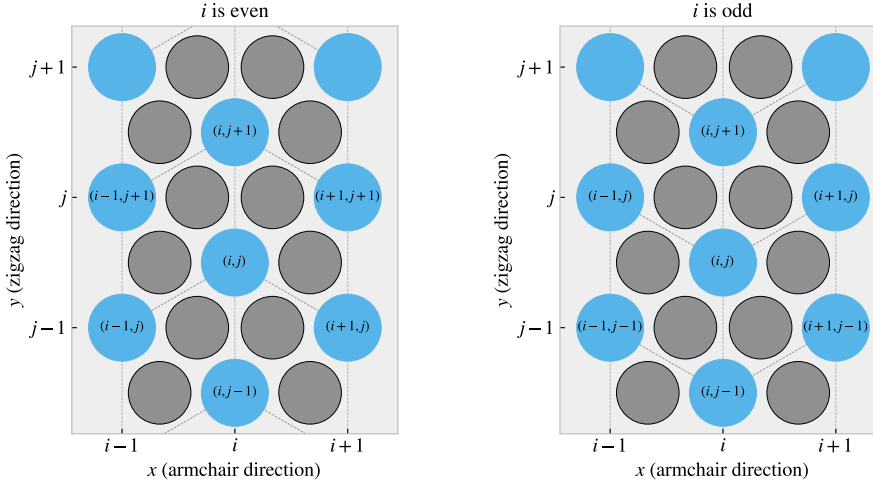


**Figure 2.6:** Graphene center elements directions

We define a cut pattern by connecting center elements into connected paths. As we walk element to element we remove atoms according to one of two rules

1. Remove intersection atoms: We remove the pair of atoms placed directly in the path we are walking. That is, when jumping to the “up” center element we remove the two upper atoms located in the local hexagon of atoms. This method is sensitive to the order of the center elements in the path.
2. Remove all surrounding atoms: We simply remove all atoms in the local hexagon surrounding each center element. This method is independent of the ordering of center elements in the path.

We notice that removing atoms using either of these rules will not guarantee an unique cut pattern. Rule 1 is the more sensitive to paths but we realize that, for an even  $i$ , we will remove the same five atoms following

either of the following paths.

$$(i, j) \rightarrow \underbrace{(i+1, j+1)}_{\text{upper right}} \rightarrow \underbrace{(i, j+1)}_{\text{up}} \rightarrow \underbrace{(i+1, j+2)}_{\text{upperright + up}} \rightarrow \underbrace{(i+1, j+1)}_{\text{upper right}}$$

$$(i, j) \rightarrow \underbrace{(i+1, j+1)}_{\text{upper right}} \rightarrow \underbrace{(i+1, j+2)}_{\text{upperright + up}} \rightarrow \underbrace{(i, j+1)}_{\text{up}}$$

For rule 2 it is even more obvious that different paths can result in the same atoms being removed. This is the reason that we needed to define and indexing system for the atom position itself even though that all cuts generated manually will use the center element path as reference.

Illustrate some delete path?

## 2.4 Kirigami patterns

We propose a series of kirigami inspired cut patterns for the altering of the graphene sheet. We seek inspiration from macroscale patterns that showcases a considerable amount of out of plane buckling when stretched. We choose to imitate two different designs: 1) An alternating repeating series of perpendicular cuts as shown in Fig. 2.7a commonly used in studies of morphable metematerials [15]. This pattern produce surface buckling with a tetrahedron (three sided pyramid) shape when stretched. 2) A more intricate pattern shown in Fig. 2.7b which is used Scotch™ Cushion Lock™ [16] as protective wrap for items during shipping. This pattern buckles into a hexagonal honeycomb structure when stretched. In addition to the modeling of the so-called *tetrahedron* and *honeycomb* patterns we also create a series of random walk styled cut patterns.

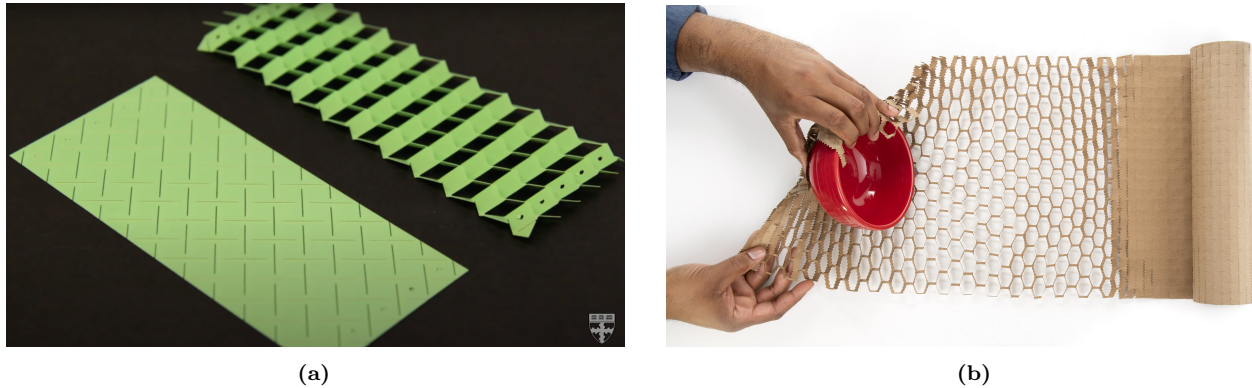


**Figure 2.7:** Macroscale kirigami cut patterns used as inspiration for the nanoscale implementation. (a) Alternating perpendicular cuts producing a tetrahedron shaped surface buckling when stretched [15]. (b) Scotch™ Cushion Lock™ [16] producing a honeycomb shaped surface buckling when stretched.

### 2.4.1 Tetrahedron

The *tetrahedron* pattern is defined in terms of center elements for which all atoms surrounding a given center element are removed. The pattern is characterized by two straight cuts, here denoted line 1 and line 2, arranged perpendicular to each other such that one line aligns with the center of the other line and with a given spacing in between. In order to achieve perpendicular cuts we cannot rely purely on the six principal directions corresponding to the center element neighbours which is spaced by  $60^\circ$ . Instead, we let line 1 run along the center elements in the direction of the “upper right” center elements (and “lower left”) while line 2 goes in the direction between the “lower” and “lower right” center elements corresponding to the direction  $(1/\sqrt{3}, -1)$ . We define variations of the pattern by the number of center elements  $L_1$  and  $L_2$  in line 1 and 2 respectively together with the spacing between the lines  $d$  as the tuple  $(L_1, L_2, d)$ . The pattern is constructed by translating the two lines to the whole sheet while according to the spacing. Due to the alignment criterias of having one line point to the center of the other line we can only have odd line length to have a clearly defined center element in the center of each line. Furthermore, in order to ensure that each translated center element stays on the same odd or even type

center element we must in practice require that  $|L_2 - L_1| = 2, 6, 10, \dots$ . In Fig. 2.8 we see a visual representation of the pattern components for the  $(7, 5, 2)$  pattern.

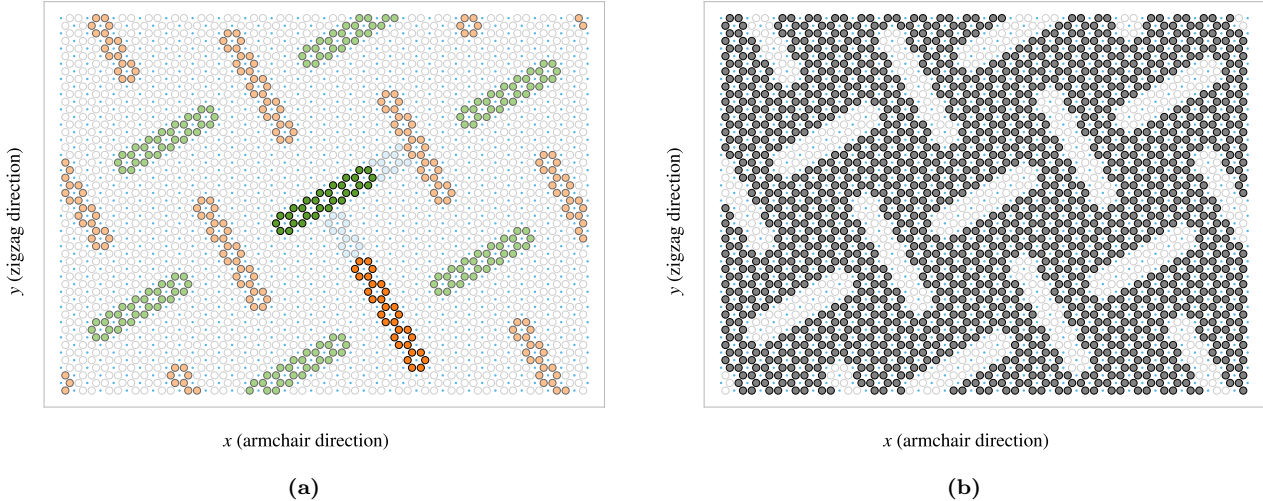


**Figure 2.8:** Visual representation of the tetrahedron pattern consisting of two perpendicular lines, line 1 and line 2, of length  $L_1$  and  $L_2$  respectively with spacing  $d$ . This example used  $(L_1, L_2, d) = (7, 5, 2)$ . (a) Highlight of the atoms removed. Line 1 is shown in green and line 2 in orange, with lighter colors for the translated variations, and the spacing is shown in light blue. (b) The sheet after applying the cut pattern where the grey circles denote atoms and the transparent white denotes removed atoms. The small blue circles show the center elements for reference

In addition to the three parameters  $L_1, L_2, d$ , the pattern is also anchored to a reference point which describes the position of line 1 and 2 before translating to the whole sheet. Due to the repeating structure of the pattern there exist a small finite number of unique reference positions. For the pattern  $(7, 5, 2)$  used as an example in Fig. 2.8 there are 140<sup>1</sup> Some additional variation of the pattern deviation from the example in Fig. 2.8 is showcased in Fig. 2.9

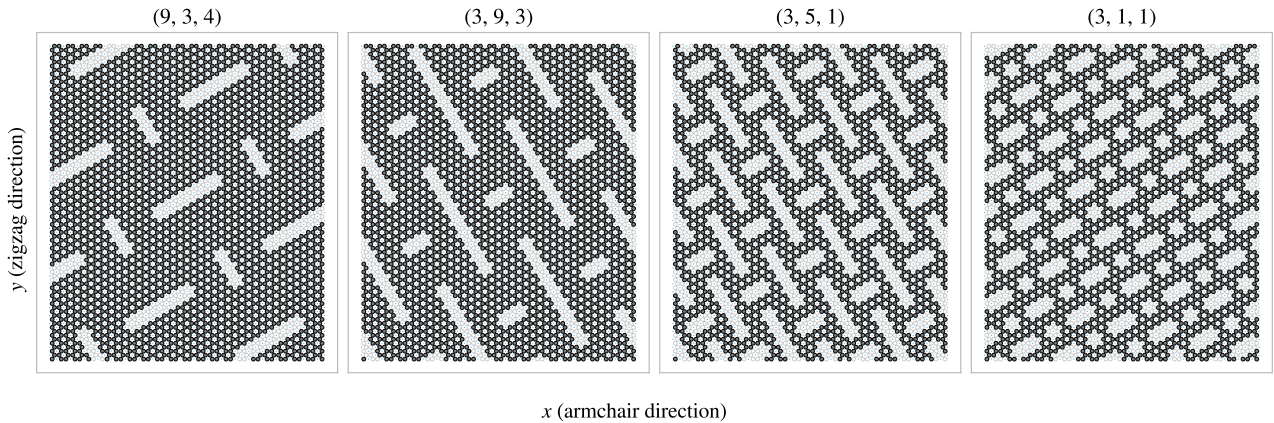


**Figure 2.9**

<sup>1</sup>The calculation of this is rather complicated in comparison of the importance in this context. Thus, we exclude the formula for this calculation as the derivation is rather handwavy and the number stated here is numerically backed for this specific parameter set.

### 2.4.2 Honeycomb

The *honeycomb* pattern is defined, similarly to the tetrahedron pattern, in terms of center elements for which all atoms surrounding a given center element are removed. The honeycomb pattern is build from a repeating series of cuts reminiscent of a roman numeral one put on its side ( $\text{I}$ ). With a given spacing these are put next to each other in the x-direction ( $\text{I}-\text{I}-\text{I}$ ) to achieve a row where only a thin *bridge* in between each cut is left to connect the sheet in the y-direction. By placing multiple rows along the y-direction with alternating x-offset we get the class of honeycomb patterns as visualized in Fig. 2.10. The pattern is described in terms of the parameters: (x-width, y-width, bridge thickness, bridge length) which is annotated in Fig. 2.10a where the parameters (2, 2, 1, 5) is used as an example. Some additional variations of the pattern class is showcased in Fig. 2.11

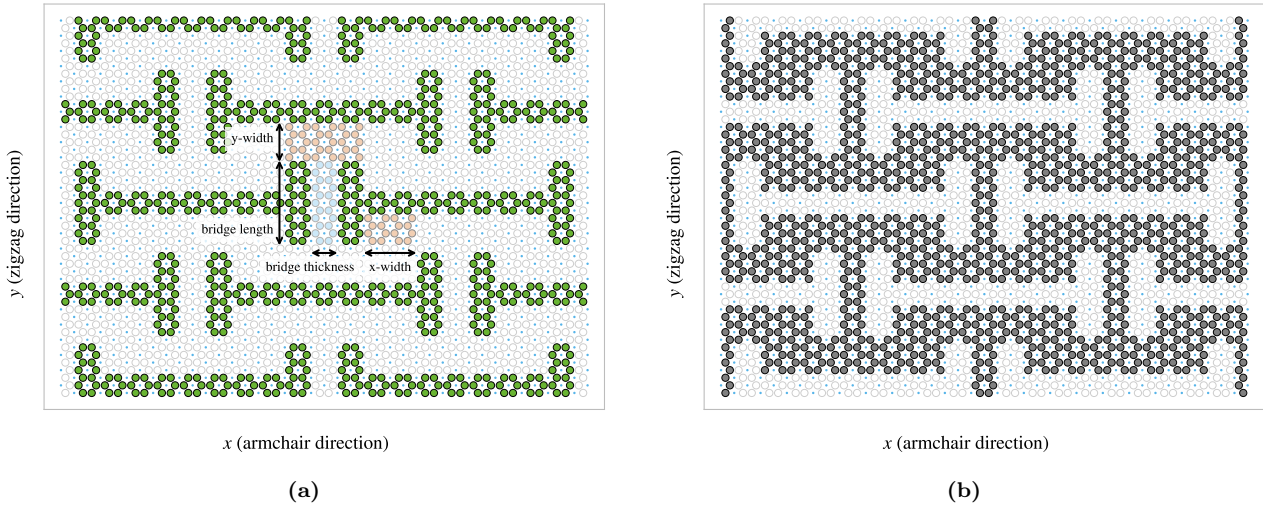


Figure 2.10

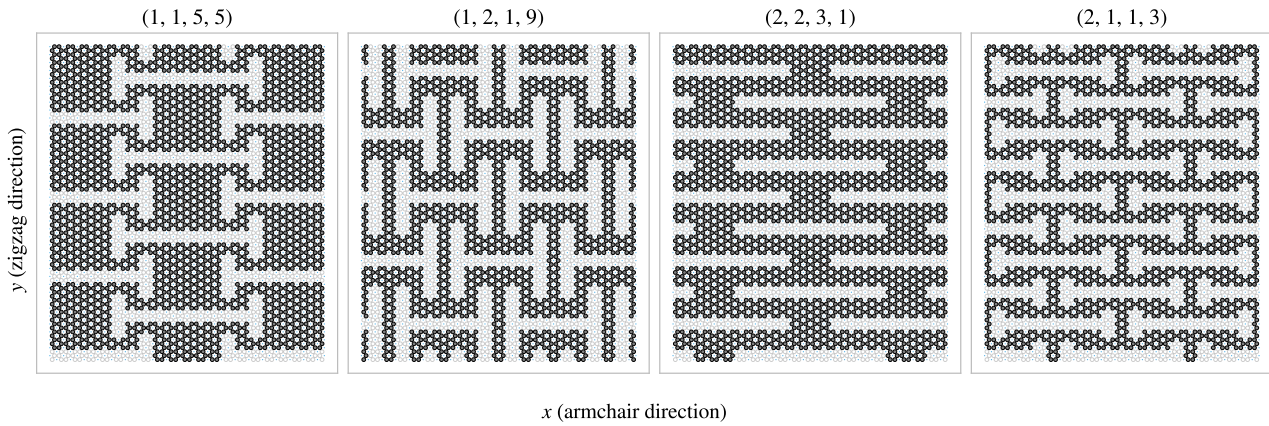


Figure 2.11

### 2.4.3 Random walk

The random walk serves as a method for introducing random patterns into the dataset with the scope of populating the configuration space more broadly than achieved with the more systematic patterns classes described above. By this argument a more straightforward way to create random configurations could be achieved by random noise, either uniform or gaussian. However, this would often leave the sheet detached with lots of non-connected atom clusters, and intuitively we do not find this promising for the generation of large scale organized structures which is hypothesized to be of interest. The random walk pattern generation is characterized by the parameters summarized in Table 2.3 which will be introduced throughout the following paragraphs.

**Table 2.3:** Parameters for the random walk generator.

| Parameters           | Value                   | Description   |
|----------------------|-------------------------|---|
| Num. walkers ( $M$ ) | Integer $\geq 1$        | Number of random walks to be initiated on the sheet (one at a time).  |
| Max. steps ( $S$ )   | Integer $\geq 1$        | The maximum steps allowed for any random walker.  |
| Min. distance        | Integer $\geq 0$        | The minimum distance required between any future paths and the previous paths in terms of the least walking steps in between.   |
| Bias                 | Vector                  | Bias direction and strength defining the discrete probability for the choice of the next site.  |
| Connection           | Atoms / Center elements | Walk between atoms or between center elements (removing all adjacent atoms).  |
| Avoid invalid        | True/False              | Whether to remove already visited sites from the neighbour list before picking the next site. This prevents jumping to already visited site and lowers the likelihood of early termination.     |
| Stay or break        | $p = [0, 1]$            |   |
| Periodic             | True/False              | Whether to use periodic boundary conditions of all four sides.  |
| Avoid clustering     | Integer $\geq 0$        | Amount of times to retry random walk in order to avoid detached clusters. Non-spanning clusters are removed after this amount of tries.   |
| RN6                  | True/False              | Randomly change the bias direction between one of the six center element directions for each random walker deployed.  |
| Grid start           | True/False              | The option to have the random walkers start in an evenly spaced grid.   |
| Centering            | True/False              | Relocate the path of a random walk after termination such that the path center of mass gets closer to the starting point (without violating the rules for travelling on already visited sites). |

#### 2.4.3.1 Fundamentals

For an uncut sheet we deploy  $M$  random walkers one at a time and let them walk for a maximum number of  $S$  steps. We can either let the walker travel between atom sites, removing the atoms in the path as it goes, or between center elements, removing all surrounding atoms - *Connection: Atom/Center elements*. Nonetheless, we will always remove a site once visited such that the walker itself or any other walker cannot use this site again. This corresponds with the property of a self avoiding random walk, but it furthermore constraint the walkers not to visit any path previously visited by another walker on the sheet. By default, the walker has an equal chance of choosing any of its adjacent neighbours for the next step, i.e. we draw the next step from a discrete uniform distribution. Optionally we can use periodic boundary conditions, *Periodic: True/False*, allowing neighbouring sites to be connected through the edge in both the x and y-direction. When traveling on atom sites this gives three neighbour options for the next step while traveling on the center elements gives six neighbour options. If the walker happens to arrive at an already visited site the walk is terminated early. Optionally, we can choose uniformly between the remaining options instead. This prolongs the walking distance. However, the walker is still able to find itself in a situation where no neighbouring sites is available, note that it cannot backtrack its own path either, and in such a case the walk is always terminated despite the setting of *Avoid invalid*.

#### 2.4.3.2 Spacing of walking paths

In order to control the spacing between the paths of the various walkers we implement a so-called *minimum distance: 0, 1, ...* parameter, describing the spacing required between paths in terms of the least amount

of steps. When a walker has ended its walk, either by early termination or hitting the maximum limits of steps, all sites within a walking distance of the minimum distance is marked as visited, although they are not removed from the sheet. This prevents any subsequent walkers to visit those sites in their walk according to the general behaviour described in the previous paragraph. In practice this is done through a recursive algorithm as described in algorithm Algorithm 1. For a given path the function `walk_distance()` is called with the input being a list of all sites in the given paths. The function will then for each site gather all site neighbours (regardless of their state on the sheet) and call itself using this neighbour list as input while incrementing a distance counter passed along. This will result in an expansion along all possible outgoing paths from the initial path of interest which is terminated when the distance counter hits the minimum distance limit. The function will then return the final neighbour lists which is cummulated into a final output corresponding to a list of all sites within the minimum distance to the path.

---

**Algorithm 1** Recursive algorithm implemented as class method to mark sites within a distance of the class attribute `self.min_dis`.

---

```

Require: self.min_dis > 0                                ▷ This pseudocode does not handle other cases
1: function WALK_DISTANCE(self, input, dis = 0, pre = [ ])      ▷ Initialize list for new neighbours
2:     new_neigh ← []
3:     for site in input do
4:         neigh ← get_neighbouring_sites(site)                  ▷ Get sourrounding neighbours
5:         for n in neigh do
6:             if (n not in pre) and (n not in new_neigh) then          ▷ If not already added
7:                 AddItem(new_neigh, n)
8:             end if
9:         end for
10:        end for
11:        dis += 1                                              ▷ Increment distance counter
12:        if dis ≥ self.min_dis then                            ▷ Max limit hit
13:            return input + new_neigh
14:        else                                                 ▷ Start a new walk from each of the neighbouring sites
15:            pre ← input
16:            return pre + self.walk_distance(new_neigh, dis, pre)
17:        end if
18:    end function

```

---

#### 2.4.3.3 Bias

We include the option perform biased random walk through the Bias: (direction, strength) parameter option. We implement this by modelling each walking step as an analog to the canonical ensemble under the influence of an external force  $\mathbf{F}$  representing the bias. For such a system each microstate  $i$ , corresponding to the sites in the neighbour list, has the associated probability  $p_i$  given by the Gibbs–Boltzmann distribution

$$p_i = \frac{1}{Z} e^{-\beta E_i}, \quad Z = \sum_i e^{-\beta E_i},$$

where  $Z$  is the canonical partition function,  $\beta = 1/k_B T$  for the boltzmann constant  $k_B$  and temperature  $T$ , and  $E_i$  the energy of site  $i$ . We model the energy of each site as the work required to move there. For a step  $\mathbf{s}$  the energy becomes  $E_i = -\mathbf{s} \cdot \mathbf{F}$ , where we notice that the energy is negative for aligned bias and step analogous to an energy gain by moving there. Due to the symmetry of both the atom sites and the center elements sites the step length to neighbouring sites will always be equal. By defining the bias magnitude  $B = \beta |\mathbf{F}| |\mathbf{s}|$  we get that the probability for jumping to site  $i$  is given by

$$p_i = \frac{1}{Z} e^{B \hat{\mathbf{s}} \cdot \hat{\mathbf{F}}} \propto e^{B \hat{\mathbf{s}} \cdot \hat{\mathbf{F}}},$$

where the hat denotes the unit direction of the vector. The bias magnitude  $B$  captures the opposing effects of the magnitude of the external force and the temperature of the system as  $B \propto |\mathbf{F}|/T$ . We notice that

$\hat{s} \cdot \hat{F} = \cos(\theta)$  for the angle  $\theta$  between the step and bias direction. This shows that the bias will have the biggest positive contribution when the step direction is aligned with the bias direction ( $\theta = 0$ ), have no contribution for orthogonal directions ( $\theta = \pm\pi/2$ ) and biggest positive contribution when the directions are antiparallel ( $\theta = \pi$ ). The partition function serves simply as a normalization constant which in practice is excluded ( $Z = 1$ ) from the calculation of  $p_i$  initially and then enforced at the final stage as a division by the sum of all  $p_i$ . In the numerical implementation we then pick the step destination weighted by the discrete probability distribution  $p_i$ . In Fig. 2.12 we have illustrated how a bias of different strength impacts the probability distribution for a random walk between center elements. We can visually confirm that the bias will favorise the directions that lies closer to the bias direction. This favorization is more distinct at high bias strengths while at low strength  $B \rightarrow 0$  we get a uniform distribution which aligns with the default unbiased random walk.

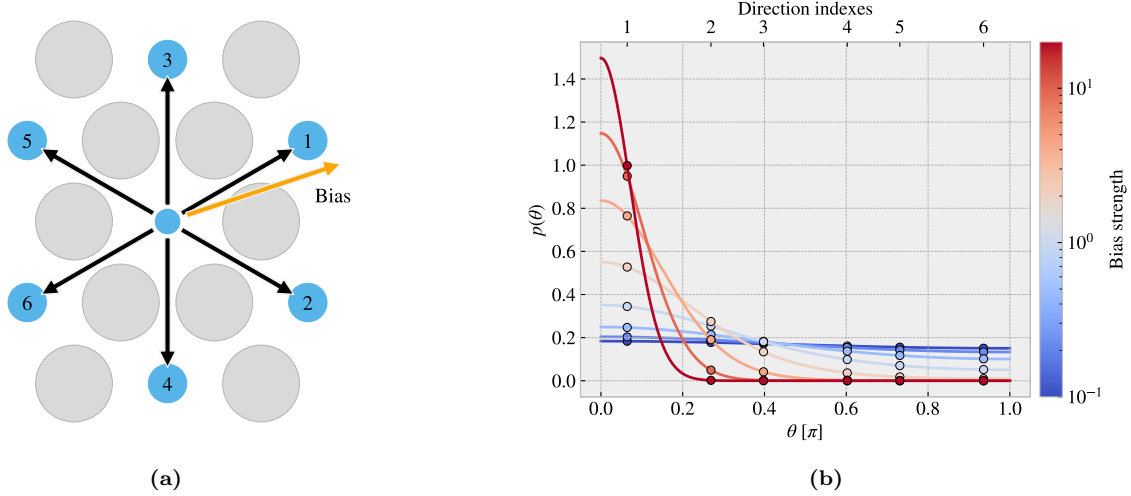


**Figure 2.12:** Illustration of the probability distribution for the various step direction during a bias random walk between center elements. (a) Shows the possible step directions as black arrows pointing towards the neighbouring center elements shown as blue circles. The bias direction is denoted as an orange arrow and the numbering indicates the most likely direction to take (1) towards the least likely (6). The atom sites are marked as grey circles for reference. (b) The probability distribution as a function of angle between the direction of choice and the bias direction. The distribution is normalized according to the discrete probabilities marked with dots for which the continuous line simply highlights the curve of the distribution. The direction indexes corresponds to the numbering on figure (a). The color map indicates different strengths of the bias.

#### 2.4.3.4 Stay or break

The *Stay or break* parameter defines the probability  $p_{\text{stay}}$  that the walker will keep its direction or otherwise break into a different direction by probability  $1 - p_{\text{stay}}$ . That is we manually substitute in the  $p_{\text{stay}}$  in the discrete probability for the direction corresponding to the direction of the last jump. We then shift the remaining probabilities such that the distribution sum to one again. In this way we can still perform bias random walk in combination. For the center element walk it is trivial to determine which of the neighbour directions correspond to the direction of the last jump. However, due to the layout of the atom sites, it is not possible to follow the same direction continuously when performing an atom site type walk. We recall that the nearest atom neighbour indexes alternates for each increment in x or y position (( $i, j$ )-index) (see eq. (2.1)) which yields alternating directions as

$$(i + j) \text{ is even} \rightarrow D = \left\{ \frac{a}{2} \left( \frac{-2}{\sqrt{3}}, 0 \right), \frac{a}{2} \left( \frac{1}{\sqrt{3}}, 1 \right), \frac{a}{2} \left( \frac{1}{\sqrt{3}}, -1 \right) \right\},$$

$$(i + j) \text{ is odd} \rightarrow D = \left\{ \frac{a}{2} \left( \frac{2}{\sqrt{3}}, 0 \right), \frac{a}{2} \left( \frac{-1}{\sqrt{3}}, 1 \right), \frac{a}{2} \left( \frac{-1}{\sqrt{3}}, -1 \right) \right\}.$$

Hence, we use the six directions from the center element walk as the common direction to stay or break from. As showcased in Fig. 2.13, for each center element direction (black arrows) there are two possible atom directions (red and orange arrows) that are equally close to the center element direction. The red and orange arrows

represent  $(i + j)$  being even or odd respectively, and we notice that these appear in pairs such that we can always determine which of the atom directions are closest to the center element direction. Following this idea we can map each center direction to an atom direction depending on the even or oddness of the position. For  $p_{\text{stay}} = 1$  this results in zigzag motion along the center element direction that happens to start on.

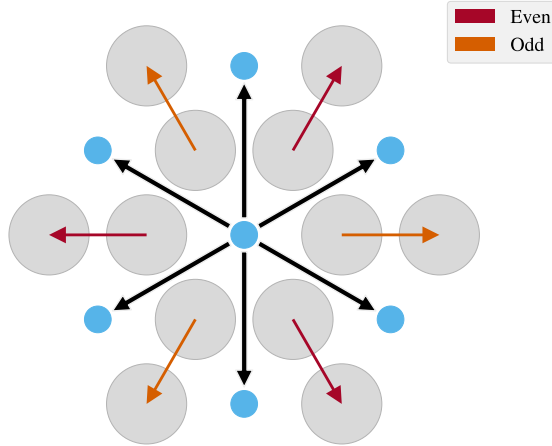


**Figure 2.13:** ...

In cases where the site corresponding to following the previous direction is not available we get a break of direction by definition.

#### 2.4.3.5 Deployment schemes

By default, each random walker is given an uniform random starting point among the non-visited sites left on the sheet. This includes any modifications in relation to the minimum distance parameter. By toggling the *Grid start: True/False* parameter on the starting points are instead predefined on evenly spaced grid. That is, the sheet is subdivided into the least amount of squares that will accomodate a space for each starting point. {1} walker leads to a  $1 \times 1$  partition, {2, 3, 4} walkers lead to a  $2 \times 2$  partition, {5, 6, 7, 8, 9} walker lead to a  $3 \times 3$  partition and so on. The lower left corner <sup>2</sup> is then choosen as a default starting place for the first walker for which the remaining sites are filled according to the order that maximizes the minimum distance between a new starting point and the ones already used. The population of the grid is visualized in Fig. 2.14 for 1-9 walkers in total.

---

<sup>2</sup>In hindsight this would have been statistically better spaced if with a random starting corner, but this is not considered to be of great importance for the way we used this feature in the dataset generation.

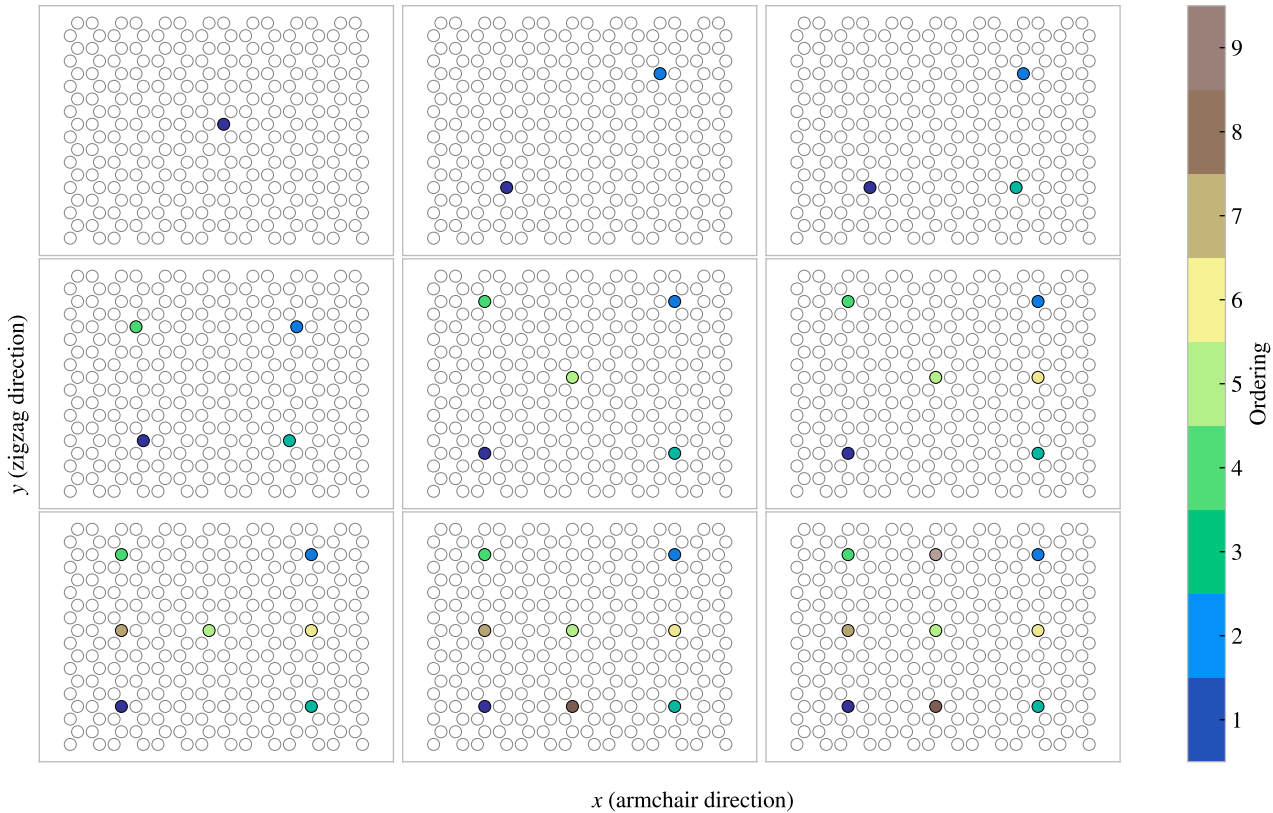


**Figure 2.14:** Population of starting points with the centering parameter toggled on in a  $14 \times 18$  sheet. This is shown for 1-9 number of random walkers with the color map conveying the order of the population.

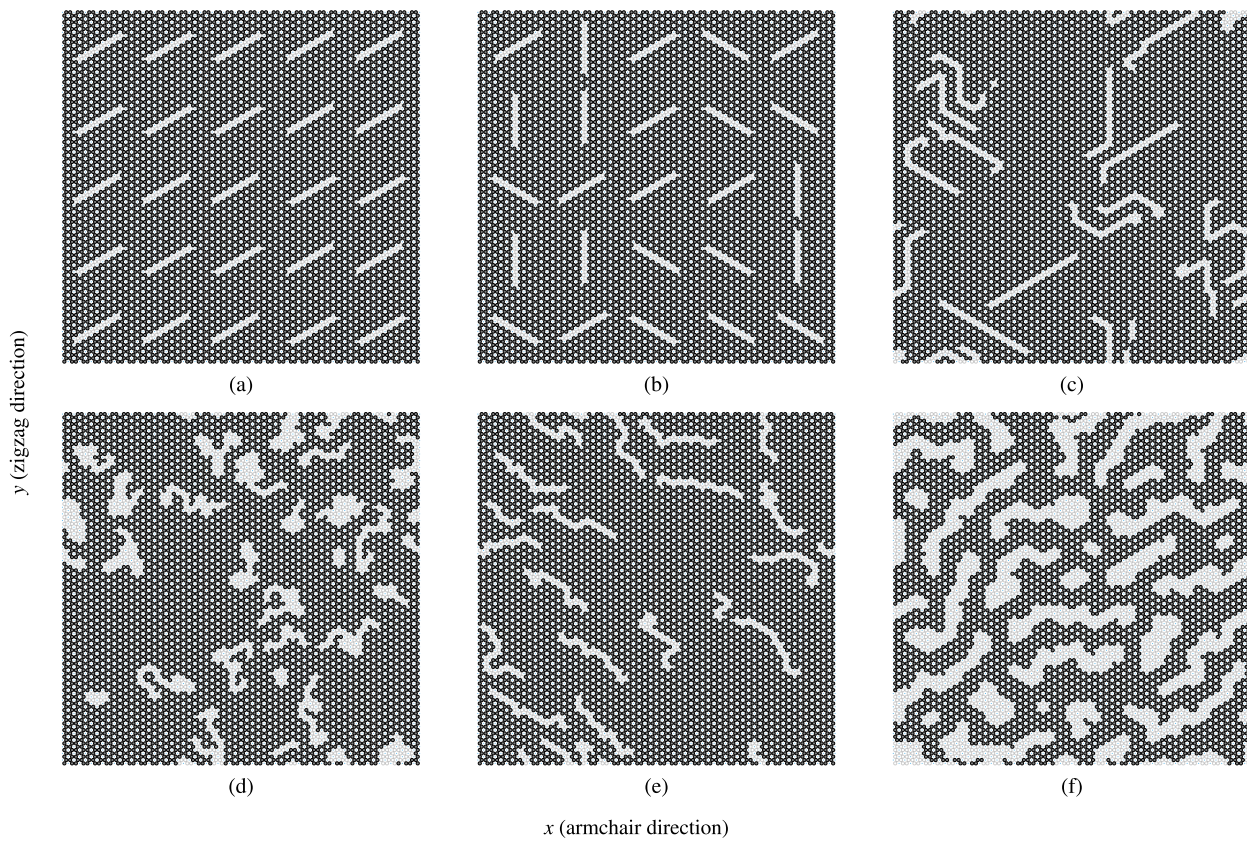
The *Centering: True/False* parameter let us relocate the path of the random walker such that the path center of mass aligns better with the starting point. This can be used in combination to the grid start and the bias parameter to make rather ordered configurations. In addition, the *RN6:True/False* parameter can be used change the bias direction to one of the six directions of the center element walk for each new walker. This lets us create configurations like [EXAMPLE].

#### 2.4.3.6 Validity

The simulation procedure requires the sheet is fully attached which can be summarized as the following requirements.

1. There exist only a single cluster on the sheet. We define a cluster as the set of atoms which can all be reached through nearest neighbour walking on the cluster.
2. The cluster of atoms is spanning the sheet in the y-direction. This means that there exist at least one path through nearest neighbour walks that connect the bottom and the top of the sheet. This is due to the reason that the sheet must be attached to the pull blocks.

In order to accommodate these requirements we count the number of clusters and search for a spanning cluster after all walkers have terminated. If the requirements are not met we simply rerun the random walk from scratch. This is done *Avoid clustering* amount of times. If the requirements are not met during any of those reruns the non-spanning clusters are simply removed. In the case of no spanning cluster the configuration is dropped. This crude scheme was later reinvented as a more refined repair scheme which alters the sheet by the intention of performing the least amount of changes (addition of subtraction of atoms) in order to meet attachment requirements. This was done as a part of the accelerated search procedure and hence it was not utilized in the creation of the random walk dataset.

**2.4.3.7 Random walk examples**

**Figure 2.15:** Some example uses of the random walking class.



# Appendices



# Appendix A



# Appendix B



# Appendix C



# Bibliography

- <sup>1</sup>E. Gnecco and E. Meyer, *Elements of friction theory and nanotribology* (Cambridge University Press, 2015).
- <sup>2</sup>Bhusnur, “Introduction”, in *Introduction to tribology* (John Wiley & Sons, Ltd, 2013) Chap. 1, 1–?
- <sup>3</sup>H.-J. Kim and D.-E. Kim, “Nano-scale friction: a review”, *International Journal of Precision Engineering and Manufacturing* **10**, 141–151 (2009).
- <sup>4</sup>K. Holmberg and A. Erdemir, “Influence of tribology on global energy consumption, costs and emissions”, *Friction* **5**, 263–284 (2017).
- <sup>5</sup>B. Bhushan, “Gecko feet: natural hairy attachment systems for smart adhesion – mechanism, modeling and development of bio-inspired materials”, in *Nanotribology and nanomechanics: an introduction* (Springer Berlin Heidelberg, Berlin, Heidelberg, 2008), pp. 1073–1134.
- <sup>6</sup>P. Z. Hanakata, E. D. Cubuk, D. K. Campbell, and H. S. Park, “Accelerated search and design of stretchable graphene kirigami using machine learning”, *Phys. Rev. Lett.* **121**, 255304 (2018).
- <sup>7</sup>P. Z. Hanakata, E. D. Cubuk, D. K. Campbell, and H. S. Park, “Forward and inverse design of kirigami via supervised autoencoder”, *Phys. Rev. Res.* **2**, 042006 (2020).
- <sup>8</sup>L.-K. Wan, Y.-X. Xue, J.-W. Jiang, and H. S. Park, “Machine learning accelerated search of the strongest graphene/h-bn interface with designed fracture properties”, *Journal of Applied Physics* **133**, 024302 (2023).
- <sup>9</sup>Y. Mao, Q. He, and X. Zhao, “Designing complex architectured materials with generative adversarial networks”, *Science Advances* **6**, eaaz4169 (2020).
- <sup>10</sup>Z. Yang, C.-H. Yu, and M. J. Buehler, “Deep learning model to predict complex stress and strain fields in hierarchical composites”, *Science Advances* **7**, eabd7416 (2021).
- <sup>11</sup>A. E. Forte, P. Z. Hanakata, L. Jin, E. Zari, A. Zareei, M. C. Fernandes, L. Sumner, J. Alvarez, and K. Bertoldi, “Inverse design of inflatable soft membranes through machine learning”, *Advanced Functional Materials* **32**, 2111610 (2022).
- <sup>12</sup>S. Chen, J. Chen, X. Zhang, Z.-Y. Li, and J. Li, “Kirigami/origami: unfolding the new regime of advanced 3D microfabrication/nanofabrication with “folding””, *Light: Science & Applications* **9**, 75 (2020).
- <sup>13</sup>Z. Deng, A. Smolyanitsky, Q. Li, X.-Q. Feng, and R. J. Cannara, “Adhesion-dependent negative friction coefficient on chemically modified graphite at the nanoscale”, *Nature Materials* **11**, 1032–1037 (2012).
- <sup>14</sup>R. W. Liefferink, B. Weber, C. Coulais, and D. Bonn, “Geometric control of sliding friction”, *Extreme Mechanics Letters* **49**, 101475 (2021).
- <sup>15</sup>L. Burrows, *New pop-up strategy inspired by cuts, not folds*, (Feb. 24, 2017) <https://seas.harvard.edu/news/2017/02/new-pop-strategy-inspired-cuts-not-folds>.
- <sup>16</sup>Scotch cushion lock protective wrap, [https://www.scotchbrand.com/3M/en\\_US/scotch-brand/products/catalog/~/Scotch-Cushion-Lock-Protective-Wrap/?N=4335+3288092498+3294529207&rtr=rud](https://www.scotchbrand.com/3M/en_US/scotch-brand/products/catalog/~/Scotch-Cushion-Lock-Protective-Wrap/?N=4335+3288092498+3294529207&rtr=rud).